ELECTROSTATICS OF COAXIAL SCHOTTKY-BARRIER NANOTUBE FIELD-EFFECT TRANSISTORS

D.L. John, *Student Member, IEEE*, L.C. Castro, J.P. Clifford and D.L. Pulfrey, *Fellow, IEEE*

Department of Electrical and Computer Engineering

University of British Columbia

Vancouver, BC V6T 1Z4, Canada

contact: davidj@ieee.org or pulfrey@ece.ubc.ca

ABSTRACT

Analytical and numerical methods are used to solve Poisson's equation for carbon nanotube field-effect transistors (FETs) with a cylindrical surrounding gate and Schottky-barrier contacts to the source and drain. The effect on the nanotube potential profile of varying the work functions of all the electrodes, and the thickness and permittivity of the gate dielectric, is investigated. From these results the general trends to be expected in the above-threshold drain current-voltage characteristics of Schottky-barrier nanotube FETs are predicted. The unusual possibility of simultaneous electron and hole contributions to the drain current is revealed. The sub-threshold characteristics are computed from a solution to Laplace's equation, and the sub-threshold slope is found to depend on gate dielectric thickness in a different manner from that in other FETs.

1 INTRODUCTION

Carbon nanotubes (CNs) are being intensively investigated as possible structures from which nanoscale transistors and logic gates might be fabricated [1, 2]. In devices where the gate electrode covers the entire length of the nanotube, transistor action is achieved by the modulation, by the gate, of the potential profile at the Schottky-barrier contact appearing at the source-tube interface [3, 4], rather than by the modulation of the channel properties, as in a traditional, silicon-like field-effect transistor [5, 6]. Here we concentrate on the coaxial

Schottky-barrier carbon nanotube field-effect transistor (SB-CNFET), in which the cylindrical gate surrounds the tube and is insulated from it by a dielectric: the basic structure is shown in Fig. 1. Whereas planar structures are currently being used experimentally [4], coaxial structures, although much more difficult to fabricate, are likely to exhibit better short-channel performance [7], and, as regards modulating the Schottky-barrier thickness via capacitative coupling between the gate and the contact [8], are likely to prove more efficient.

As a first step towards providing a model for these new devices, we examine the electrostatics of coaxial SB-CNFETs, using both analytical and numerical procedures to obtain the potential profile. Of course, the solution must be consistent with the electron and hole charge induced on the surface of the nanotube, and any inherent charge, such as that due to dopants. Although the latter are easily accommodated, they are not considered here in view of the findings that procedures previously thought to lead to doping of a nanotube are more probably serving to affect the work functions at the metal contacts to the CN [4]. Thus the nanotubes here are considered to be intrinsic. The electron and hole charge densities can be computed using the nearest-neighbour tight-binding approximation for the nanotube density of states (DOS) [9]. Results are presented here for the equilibrium situation, *i.e.*, the drain-source voltage, V_{DS}, is zero, as this is presently the only case for which the carrier distribution functions are known with certainty. The dependence of the potential profile along the tube on the work functions of the source-, drain- and gate-metallizations, and of the thickness and permittivity of the gate dielectric, is reported. Outside of equilibrium, *i.e.*, for $V_{DS} \neq 0$, the distribution functions are likely to be highly distorted from their equilibrium shape [10]. This is due to the absence of thermalizing collisions in this one-dimensional (1-D) system, for which there is very little carrier-phonon interaction [11]. Presently, the only way to obtain exact results for $V_{DS} \neq 0$ is to solve Laplace's equation. This may be appropriate for studying sub-threshold conduction. Such results are presented here and they indicate a sub-threshold slope which depends on dielectric thickness in a different manner from that recently reported for planar-geometry SB-CNFETs [12].

Although, as stressed above, a procedure for obtaining a fully self-consistent solution for the above-threshold case is not yet available, the results presented here for the equilibrium

potential profiles can be used to infer the general form of the drain current-voltage (I-V) characteristic. On doing this, the interesting spectre of having simultaneous injection of electrons and holes into the nanotube is raised. The drain characteristics for such a situation are briefly examined using a rudimentary, non-equilibrium, compact model [10], in which the source and drain potential profiles are approximated by exponential expressions that have their basis in the electrostatic solutions presented herein.

2 COAXIAL NANOTUBE ELECTROSTATICS

The electrostatic problem reduces to that of a bounded cylinder of length L and radius R_G, as shown in Fig. 1. In cylindrical coordinates, using the source electrode as reference, the appropriate boundary conditions for the potential $V(\rho, \phi, z)$ are:

$$\begin{aligned} V(R_G, \phi, z) &= V_{GS} - \Phi_G/q \\ V(\rho, \phi, 0) &= -\Phi_S/q \\ V(\rho, \phi, L) &= V_{DS} - \Phi_D/q \\ V(\rho, \phi, z) &= V(\rho, \phi + 2\pi, z)\,, \end{aligned} \tag{1}$$

where Φ_G, Φ_S and Φ_D are the work functions of the gate-, source- and drain-metallizations, respectively, V_{GS} is the gate-source voltage, and q is the magnitude of the electronic charge. The boundary conditions at $z = 0$ and $z = L$ are appropriate in the absence of Fermi-level pinning [13]. Note, too, that $V(0, \phi, z)$ is assumed to be finite.

An analytical solution, at least for the case of a homogeneous permittivity within the metallized enclosure, is possible following the methods of [14] and [15]. Such a procedure is described in the Appendix. For the inhomogeneous case of different permittivities for the dielectric and the nanotube, numerical techniques are easier to implement. We have used a standard finite-element package for this purpose[1].

The net carrier density, comprising electrons and holes, is taken to reside on the surface of the CN, and is given by

$$Q(\mathbf{r}') = \frac{1}{2\pi\rho'}\delta(\rho' - R_T)Q_z(z')\,, \tag{2}$$

[1]FEMLAB, see *http://www.comsol.com*

where $Q_z(z')$ is the net 1-D carrier concentration, R_T is the CN radius, and $\delta(x)$ is the Dirac delta function. The nanotube charge needs to be computed self-consistently with the potential on the nanotube but, as mentioned in the Introduction, a difficulty arises under non-equilibrium conditions because of the present inability to rigorously specify the distribution function for the hot carriers within the tube. However, for equilibrium conditions, there is no such problem and the carrier concentrations are found by allowing the local electrostatic potential to rigidly shift the CN DOS [14, 15]. Using the nearest-neighbour tight-binding approximation [9], the DOS is symmetrical about E_F, so the net 1-D carrier density at some point along the intrinsic tube may be computed as

$$Q_z(z') = \int_0^\infty g(E) \left[f(E + qV') - f(E - qV') \right] \mathrm{d}E \,, \tag{3}$$

where $g(E)$ is the 1-D tube DOS, the degeneracy in the energy bands is as considered in [17], $f(E)$ is the Fermi-Dirac distribution function, E_F is taken to be zero, and $V' = V + \Phi_{CN}/q$, where Φ_{CN} is the work function of the intrinsic carbon nanotube.

For the non-equilibrium case, the only exact solution that can be given presently is for the case of no charge on the nanotube, namely: $Q_z(z') = 0$. A complete solution awaits the formulation of an appropriate solver, likely of the Poisson-Schrödinger variety.

3 RESULTS AND DISCUSSION

Results are presented for $(16, 0)$ tubes having a radius of 0.63 nm, a length of 100 nm and a gate work function of 4.5 eV. Various ratios of gate radius to tube radius, relative permittivity of the dielectric, $\epsilon_{r,d}$, and source- and drain-work functions, are considered. The electron affinity for the carbon nanotube is taken to be 4.18 eV, based on a work function of 4.5 eV [16], and an intrinsic-tube band gap of 0.64 eV. Unless otherwise stated, the relative permittivity of the nanotube, $\epsilon_{r,CN}$, is taken to be the same as that of the gate dielectric. The temperature is taken to be 300 K.

At equilibrium conditions, and when $\Phi_S = \Phi_D$, the potential profile along the tube will be symmetrical. Thus, only profiles near one contact need be shown. Fig. 2 shows the energy band diagrams near the source for $R_G/R_T = 10$, $\epsilon_{r,d} = 3.9$ and for various $\Phi_S = \Phi_D$ with

$V_{DS} = 0\,\mathrm{V}$ and $V_{GS} = 0.2$ and $0.5\,\mathrm{V}$. In Fig. 2(a), $\Phi_S = 4.5\,\mathrm{eV}$ and corresponds to the case of equal work functions for the metal and the nanotube, whereas $\Phi_S = 4.33\,\mathrm{eV}$ [Fig. 2(b)] and $\Phi_S = 4.63\,\mathrm{eV}$ [Fig. 2(c)] refer to low- and high-metal work functions, respectively [13]. The potential in the body of the tube, distal from the contacts, depends directly on V_{GS}, leading to potential spikes in the tube at the source and drain of height determined by both $\Phi_{S,D}$ and V_{GS}. Only in the low-Φ_S case at low V_{GS} is thermionic emission likely to make a significant contribution to the source current. In all other cases shown in Fig. 2, tunneling of electrons through the spike will dominate.

The band diagrams for the same work function cases as used in Fig. 2, but for $R_G/R_T = 50$, are shown in Fig. 3. The reduced band bending in the tube at the contacts, due to poorer coupling between the gate and the nanotube, is very evident, and will lead to a dramatic decrease in current, except in the low work function case at low V_{GS} where, as mentioned previously, the electron current will be due to thermionic emission and will be determined by the height, and not the shape, of the barrier. The present state of the art as regards gate-dielectric thinness is 2 nm [12]. Regarding the permittivity of the dielectric, recent work has reported the use of zirconia [6], for which $\epsilon_{r,d}$ is around 5 times higher than that used in obtaining the above figures. The effect of such a change in $\epsilon_{r,d}$ can be seen by comparing Figs. 2 and 4. At $V_{GS} = 0.5\,\mathrm{V}$, the increased capacitative coupling between the gate and the tube drives the mid-tube potential energy to lower values, yet does not change significantly the width of the source barrier at its base. Thus, obviously, an increased current for a given bias will result from using a higher $\epsilon_{r,d}$. At lower V_{GS}, *e.g.,* $0.2\,\mathrm{V}$, the increased $\epsilon_{r,d}$ makes essentially no difference to the potential profile because, at least for $R_G/R_T = 10$, there is virtually no charge induced on the tube. From Figs. 2, 3 and 4, it appears that the width of the potential barrier at its base depends strongly on the radius of the gate R_G for the contact geometry considered here, as has been remarked upon elsewhere [18], and here we indicate that it also depends barely at all on V_{GS}.

Note that the effect of changing the gate work function from the value of $4.5\,\mathrm{eV}$ used here can be readily appreciated from the foregoing figures as an increase in Φ_G of $0.1\,\mathrm{eV}$, for example, has the same effect as a corresponding decrease in V_{GS}.

Turning now to the non-equilibrium case, as mentioned above, only the case of zero charge on the nanotube can be solved for exactly, pending the determination of the appropriate distribution functions or wave-functions for the hot carriers. In sub-threshold, the charge accumulation is not significant in the electrostatics solution, thus, we solve Laplace's equation in order to study the behaviour in this regime [12]. The current is computed from the Landauer-Büttiker formula, assuming ballistic transport and incorporating the effect of carrier transmission and reflection at the internal source/tube- and drain/tube-barriers in the WKB-computed transmission coefficient, T,

$$I = \frac{4q}{h} \int T(E)[f(E) - f(E - qV_{DS})]\, dE\,. \tag{4}$$

Some results for various gate/tube dimensions are shown in Fig. 5: note that the dielectric thickness is $t_d = R_G - R_T$. The sub-threshold current can be due to either mainly electrons or mainly holes, depending on the bias conditions. For $V_{DS} = 0.1\,\mathrm{V}$, as used in obtaining Fig. 5, at $V_{GS} = 0$ there is no band bending at the source end of the tube, but there is a "spike" in the valence band at the drain end of the tube, which permits a hole tunneling current. This current increases as V_{GS} becomes more negative. For positive values of V_{GS}, a spike appears in the conduction band at the source, thereby allowing electron tunneling, but the spike in the valence band at the drain thickens, and so the hole current is reduced. These changes with V_{GS} lead to a minimum in current, which occurs at $V_{GS} = V_{DS}/2$, when the tunneling barriers for source electrons and drain holes are of equal thickness. The magnitudes of the sub-threshold slopes, $|S| = |(d \log_{10} I/dV_{GS})^{-1}|$, for both mainly electron conduction ($V_{GS} > V_{DS}/2$), and mainly hole conduction ($V_{GS} < V_{DS}/2$), are identical, owing to the use here of a symmetrical DOS function for the conduction- and valence-bands, and equal work functions for the source and drain contacts.

In analyzing their planar SB-CNFETs, Heinze *et al.* [12] noted that changing the dielectric thickness is equivalent to rescaling the gate voltage. Thus, they found that S and the tube potential scaled with dielectric thickness in the same manner, *i.e.*, as $\sqrt{t_d}$. This suggests that we seek a scaling relationship for S in our coaxial devices by examining how the V_{GS}-dependent part of the potential in the vicinity of the source contact varies with t_d. This can be accomplished by expanding the first term of the first mode of the Laplace solution from

(8), *i.e.*,

$$V \simeq \frac{4(qV_{GS} - \Phi_G)\mathrm{I}_0\left(\frac{\pi R_T}{L}\right)\frac{\pi z}{L}}{q\pi \mathrm{I}_0\left(\frac{\pi R_G}{L}\right)}\,, \tag{5}$$

where I_0 is the zeroth-order Modified Bessel Function of the First Kind. Thus,

$$\frac{\partial V}{\partial V_{GS}} \propto \frac{1}{\mathrm{I}_0\left(\frac{\pi R_G}{L}\right)}\,, \tag{6}$$

and, therefore, we can expect

$$S \simeq \alpha \mathrm{I}_0(\beta t_d)\,, \tag{7}$$

where α and β are fitting parameters. It is found that a reasonable fit to S, from the data included in Fig. 5, results with $\alpha \approx 79\,\mathrm{mV/decade}$ and $\beta \approx 0.15\,\mathrm{nm}^{-1}$. The fact that a fit can be obtained confirms that the dependence of S on t_d is related to the specific geometry of the transistor, with a Bessel function being involved in this case because of the cylindrical structure. Electrically, t_d is related, of course, to the gate capacitance, through which V_{GS} is coupled to the CN potential.

Considering now the case of above-threshold conduction, the solution to Laplace's equation for various values of V_{DS} is worth examining as it gives an idea of the evolution of the barrier profiles with drain-source voltage. The exact solutions for the drain end of the tube show that the conduction-band spike diminishes with V_{DS}, and that, on further increasing V_{DS}, a spike occurs in the valence band. The base widths of the potential profiles at both source and drain are found, as in the equilibrium case, to be of the order of R_G. This fact has been used, in conjunction with a self-consistent procedure for solving for the potential and the charge in the mid-length, field-free region of the tube, to generate compact expressions which describe the potential along the entire length of the tube as a function of V_{GS} and V_{DS} [10].

Results are shown in Fig. 6 for the SB-CNFET for which the equilibrium band diagram is shown in Fig. 2(a). As mentioned, the barrier at the drain for electron flow from the nanotube into the drain diminishes as V_{DS} is increased. This will lead to reduced reflection of source-injected electrons and an increase, and eventual saturation, of the electron current. Further increase in V_{DS} causes a spike to appear in the valence band profile at the drain. This will allow hole tunneling to occur, and raises the interesting prospect of a hole current issuing

from the drain contact and adding to the electron current, thereby leading to a significant increase in the total drain current. When the electron current is small due to the absence of a tunneling barrier at the source, as will occur at low V_{GS}, the drain current will be due almost entirely to holes, and the drain I-V characteristic will appear near-exponential in shape.

An illustrative drain *I-V* characteristic is shown in Fig. 7. This data is generated from the compact model of Castro *et al.* [10], as used to produce the potential profiles in Fig. 6, with the base width of the potential barriers being taken as equal to $2R_G$. Castro's model is based on that of Guo *et al.* [5], and improves upon it by: introducing Schottky barrier contacts at the source and drain; accounting for reflection of carriers in the tube between the source and drain barriers; allowing for simultaneous electron and hole flows; and not demanding that the charge in the mid-length tube region remain at its equilibrium value. It is an approximate model due to the estimated shape of the barrier profiles, so the current magnitudes given in Fig. 7 are also only approximate. However, they do confirm the evolution of the drain characteristics, as inferred from the above discussion of the exact potential profiles displayed in the present work. Furthermore, our predictions are consistent with very recent experimental results that show near-exponential drain *I-V* characteristics for $V_{GS} < V_{DS}$ [19].

As a final comment on the simultaneous presence of electrons and holes in the nanotube, some recombination is to be expected, in which case the drain current will be less than the sum of two non-interacting particle flows, and in practice may not increase as dramatically as indicated here. Experimentally, evidence of recombination within the nanotube of a SB-CNFET has been demonstrated via the measurement of light emission under bias conditions appropriate for the simultaneous injection of holes and electrons [19].

4 CONCLUSIONS

From this work on the electrostatics of coaxial Schottky-barrier carbon nanotube FETs it can be concluded that:

1. the potential barriers at the source/nanotube- and drain/nanotube-interfaces are strongly affected by the work functions of the source, drain and gate, and by the thickness and permittivity of the dielectric that surrounds the nanotube;

2. an analytical solution for the potential distribution in the case of equal permittivities of the gate dielectric and the nanotube gives a good approximation to the numerical solution for the case when the difference in permittivities of the dielectric and tube is taken into account. In other words, the radial field inside the nanotube, for this particular geometry, is not of great importance;

3. the sub-threshold slope approaches the thermionic limit of $\approx 60\,\mathrm{mV/decade}$ as the dielectric thickness is reduced, in a manner consistent with the cylindrical geometry of the device;

4. from the results presented here, trends in the above-threshold drain I-V characteristics can be inferred. The possibility of contributions to the drain current from both electron and hole flow is indicated.

References

[1] V. Derycke, R. Martel, J. Appenzeller, and Ph. Avouris, "Carbon nanotube inter- and intramolecular logic gates," *Nano Lett.*, vol. 1, no. 9, pp. 453–456, 2001.

[2] A. Bachtold, P. Hadley, T. Nakanishi, and C. Dekker, "Logic circuits with carbon nanotube transistors," *Science*, vol. 294, pp. 1317–1320 , 2001.

[3] S. Heinze, J. Tersoff, R. Martel, V. Derycke, J. Appenzeller, and Ph. Avouris, "Carbon nanotubes as Schottky barrier transistors," *Phys. Rev. Lett.*, vol. 89, no. 10, pp. 106801-1–106801-4, 2002.

[4] J. Appenzeller, J. Knoch, V. Derycke, R. Martel, S. Wind, and Ph. Avouris, "Field-modulated carrier transport in carbon nanotube transistors," *Phys. Rev. Lett.*, vol. 89, no. 12, pp. 126801-1–126801-4, 2002.

[5] J. Guo, M. Lundstrom, and S. Datta, "Performance projections for ballistic carbon nanotube field-effect transistors," *Appl. Phys. Lett.*, vol. 80, no. 17, pp. 3192–3194, 2002.

[6] A. Javey, H. Kim, M. Brink, Q. Wang, A. Ural, J. Guo, P. McIntyre, P. McEuen, M. Lundstrom and H. Dai, "High-κ dielectrics for advanced carbon-nanotube transistors and logic gates," *Nature Materials*, vol. 1, pp. 241–246, 2002.

[7] S.-H. Oh, D. Monroe, and J.M. Hergenrother, "Analytic description of short-channel effects in fully-depleted double-gate and cylindrical, surrounding-gate MOSFETs", *IEEE Electron Dev. Lett.*, vol. 21, no. 9, pp. 445–447, 2000.

[8] B. Winstead and U. Ravaioli, "Simulation of Schottky barrier MOSFET's with a coupled quantum injection/Monte Carlo technique," *IEEE Trans. Electron Dev.*, vol. 47, no. 6, pp. 1241–1246, 2000.

[9] K. Esfarjani, A.A. Farajian, Y. Hashi, and Y. Kawazoe, in *Clusters and Nanomaterials—Theory and Experiment*, edited by Y. Kawazoe, T. Kondow, and K. Ohno, (Springer-Verlag, Berlin, 2002), Chap. 8, pp. 187–220.

[10] L.C. Castro, D.L. John, and D.L. Pulfrey, "Towards a compact model for Schottky-barrier nanotube FETs," *Proc. IEEE COMMAD*, Sydney, Australia, 2002, accepted for publication April 7, 2003. Draft available at *www.ece.ubc.ca/∼pulfrey*

[11] P.L. McEuen, M.S. Fuhrer, and H. Park, "Single-walled carbon nanotube electronics," *IEEE Trans. Nanotechnology*, vol. 1, no. 1, pp. 78–85, 2002.

[12] S. Heinze, M. Radosavljević, J. Tersoff and Ph. Avouris, "Unexpected scaling of the performance of carbon nanotube transistors", *arXiv:cond-mat/0302175 v1*, 10 Feb 2003.

[13] F. Léonard and J. Tersoff, "Role of Fermi-level pinning in nanotube Schottky diodes," *Phys. Rev. Lett.*, vol. 84, no. 20, pp. 4693–4696, 2000.

[14] F. Léonard and J. Tersoff, "Novel length scales in nanotube devices," *Phys. Rev. Lett.*, vol. 83, no. 24, pp. 5174–5177, 1999.

[15] A.A. Odintsov, "Schottky barriers in carbon nanotube heterojunctions," *Phys. Rev. Lett.*, vol. 85, no. 1, pp. 150–153, 2000.

[16] S.J. Tans, A.R.M. Verschueren, and C. Dekker, "Room-temperature transistor based on a single carbon nanotube," *Nature*, vol. 393, pp. 49–52, 1998.

[17] M.S. Dresselhaus, G. Dresselhaus, and P.C. Eklund, *Science of Fullerenes and Carbon Nanotubes*. Toronto: Academic Press, 1996.

[18] T. Nakanishi, A. Bachtold, and C. Dekker, "Transport through the interface between a semiconducting carbon nanotube and a metal electrode," *Phys. Rev. B*, vol. 66, pp. 073307-1–073307-4, 2002.

[19] J.A. Misewich, R. Martel, Ph. Avouris, J.C. Tsang, S. Heinze, and J. Tersoff, "Electrically induced optical emission from a carbon nanotube FET," *Science*, vol. 300, pp. 783–786, 2003.

[20] J.D. Jackson, *Classical Electrodynamics*. Toronto: John Wiley and Sons, 3rd ed., 1999.

Appendix: An Analytical Solution for the Potential

An analytical solution of the electrostatic problem posed by the structure of Fig. 1 is straightforward, at least in the homogeneous case of equal permittivities of the gate dielectric and the nanotube, and is achieved by superposition of the solutions to two cases:

1. Laplace's equation using the contact boundary conditions, for which the solution is most easily obtained by solving for $V_{DS} = 0$ and $V_{GS} = 0$ separately; and

2. Poisson's equation using homogeneous boundary conditions, for which the solution is readily obtained via the Green's function formalism.

The solution to the first case is

$$V = \sum_{n=1}^{\infty} \left[\mathrm{A}_n \mathrm{I}_0\left(\tfrac{n\pi\rho}{L}\right) \sin\left(\tfrac{n\pi z}{L}\right) + \mathrm{B}_n \mathrm{J}_0\left(\tfrac{x_{0n}\rho}{R_G}\right) \sinh\left(\tfrac{x_{0n} z}{R_G}\right) + \mathrm{C}_n \mathrm{J}_0\left(\tfrac{x_{0n}\rho}{R_G}\right) \sinh\left(\tfrac{x_{0n}(L-z)}{R_G}\right) \right] , \tag{8}$$

where

$$\mathrm{A}_n = \frac{2(qV_{GS} - \Phi_G)(1-(-1)^n)}{qn\pi \mathrm{I}_0\left(\tfrac{n\pi R_G}{L}\right)} \tag{9}$$

$$\mathrm{B}_n = \frac{2\left(qV_{DS} - \Phi_D\right)}{qx_{0n} \sinh\left(\tfrac{x_{0n}L}{R_G}\right) \mathrm{J}_1(x_{0n})} \tag{10}$$

$$\mathrm{C}_n = -\frac{2\Phi_S}{qx_{0n} \sinh\left(\tfrac{x_{0n}L}{R_G}\right) \mathrm{J}_1(x_{0n})} , \tag{11}$$

$\mathrm{J}_m(x)$ and $\mathrm{I}_m(x)$ are the Bessel Function and Modified Bessel Function, respectively, of the First Kind of Order m, and x_{mn} is the nth solution to $\mathrm{J}_m(x) = 0$.

The appropriate Green's function for the second case, noting the angular symmetry in the problem, is [20]

$$G(\mathbf{r};\mathbf{r}') = \frac{-2}{\pi L R_G^2} \sum_{n=1}^{\infty} \sum_{l=1}^{\infty} \frac{\mathrm{J}_0\left(\tfrac{x_{0l}\rho}{R_G}\right) \mathrm{J}_0\left(\tfrac{x_{0l}\rho'}{R_G}\right) \sin\left(\tfrac{n\pi z}{L}\right) \sin\left(\tfrac{n\pi z'}{L}\right)}{\mathrm{J}_1^2\left(x_{0l}\right) \left[\left(\tfrac{x_{0l}}{R_G}\right)^2 + \left(\tfrac{n\pi}{L}\right)^2 \right]} \tag{12}$$

with the total solution for this case given by

$$V(\mathbf{r}) = -\frac{q}{\epsilon} \int Q(\mathbf{r}') G(\mathbf{r};\mathbf{r}') \, \mathrm{d}^3 r' , \tag{13}$$

where the integral is over the entire volume of the device, and ϵ is the permittivity.

The errors involved in assuming a homogeneous permittivity within the metal-bounded space can be computed by comparing results from the above analytical analysis with those from a numerical, finite-element analysis in which different permittivities for the gate dielectric and nanotube are taken into account. For a $(16, 0)$ tube with $R_G/R_T = 10$, all metal work functions equal to $4.5\,\mathrm{eV}$, $\epsilon_{r,d} = 3.9$ and $\epsilon_{r,CN} = 1.0$, the discrepancy between the predicted potential profiles increases with V_{GS} and reaches about 2% for a bias of $V_{GS} = 0.5\,\mathrm{V}$, for example. This discrepancy is only appreciable in the regions very close ($\approx 5\,\mathrm{nm}$) to the source and drain contacts, as it is only here that a significant radial field exists within the tube due to field lines from the gate terminating on the small portions of the source/drain electrodes that actually cap the circular cross-section of the tube. For $\epsilon_{r,d} = 19.5$, this error rises to about 3% at $V_{GS} = 0.5\,\mathrm{V}$. The homogeneous-permittivity analytical solution overestimates the width of the potential barriers at the source and drain and, therefore, will lead to an understimation of the current.

List of Figures

1 SB-CNFET model geometry. The gate forms the curved surface of the outer cylinder, and the source and drain form the two ends. The semiconducting nanotube is placed coaxially with the outer cylinder. 16

2 Self-consistent equilibrium energy band diagram near the source for a $(16, 0)$ tube with a 5.6 nm gate dielectric thickness ($R_G/R_T = 10$), and $\Phi_S = \Phi_D$ set to (a) 4.5 eV, (b) 4.33 eV, and (c) 4.63 eV. Data are for $V_{DS} = 0$ V and $V_{GS} = 0.2$ (dashed line) and 0.5 V (solid line). Energies are with respect to the Fermi level (dotted line). 17

3 Self-consistent equilibrium energy band diagram near the source for a $(16, 0)$ tube with a 30.9 nm gate dielectric thickness ($R_G/R_T = 50$), and the same sequence of work functions as in Fig. 2, namely: $\Phi_S = \Phi_D$ set to (a) 4.5 eV, (b) 4.33 eV, and (c) 4.63 eV. Data are for $V_{DS} = 0$ V and $V_{GS} = 0.2$ (dashed line) and 0.5 V (solid line). Energies are with respect to the Fermi level (dotted line). 18

4 Self-consistent equilibrium energy band diagram near the source for a $(16, 0)$ tube with a 5.6 nm gate dielectric thickness ($R_G/R_T = 10$), a gate dielectric with permittivity 5 times higher than used in Fig. 2, and the same sequence of work functions as in Fig. 2, namely: $\Phi_S = \Phi_D$ set to (a) 4.5 eV, (b) 4.33 eV, and (c) 4.63 eV. Data are for $V_{DS} = 0$ V and $V_{GS} = 0.2$ (dashed line) and 0.5 V (solid line). Energies are with respect to the Fermi level (dotted line). 19

5 Sub-threshold current for the same tube properties as in Fig. 2(a), but with various ratios of gate radius to tube radius, for $V_{DS} = 0.1$ V. Note: the dielectric thickness is $R_G - R_T$. 20

6 Energy band diagrams for the same tube properties as in Fig. 2(a) for $V_{GS} = 0.3$ V and various V_{DS}: 0 V (dotted), 0.2 V (dashed), 0.5 V (solid). For the equilibrium case the profile is the exact solution of Poisson's equation; for $V_{DS} \neq 0$ the solutions are from Castro's compact model [10], with the base widths of the potential profiles at the source and drain being taken as $2R_G$. . . 21

7 Drain I-V characteristics, as calculated by the method of Ref. [10], for a $(16, 0)$ tube, $R_G/R_T = 10$, $\Phi_S = \Phi_D = 4.5\,\mathrm{eV}$ and various values of V_{GS}: $0\,\mathrm{V}$ (dotted), $0.2\,\mathrm{V}$ (dot-dashed), $0.4\,\mathrm{V}$ (dashed), $0.5\,\mathrm{V}$ (solid). 22

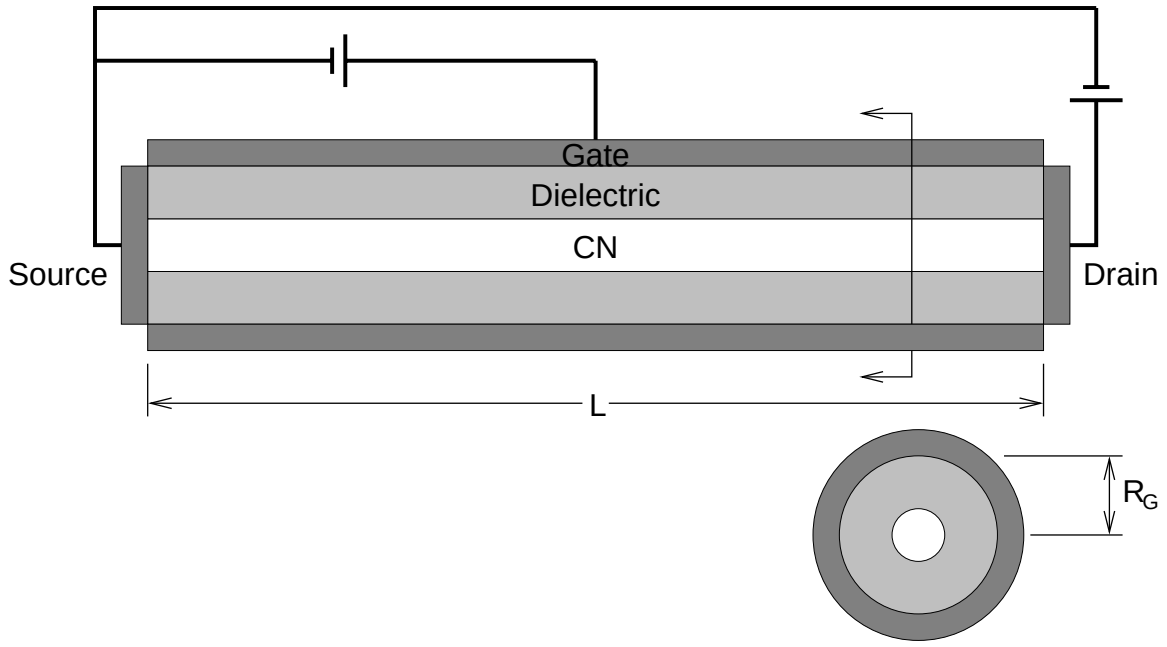

Figure 1: SB-CNFET model geometry. The gate forms the curved surface of the outer cylinder, and the source and drain form the two ends. The semiconducting nanotube is placed coaxially with the outer cylinder.

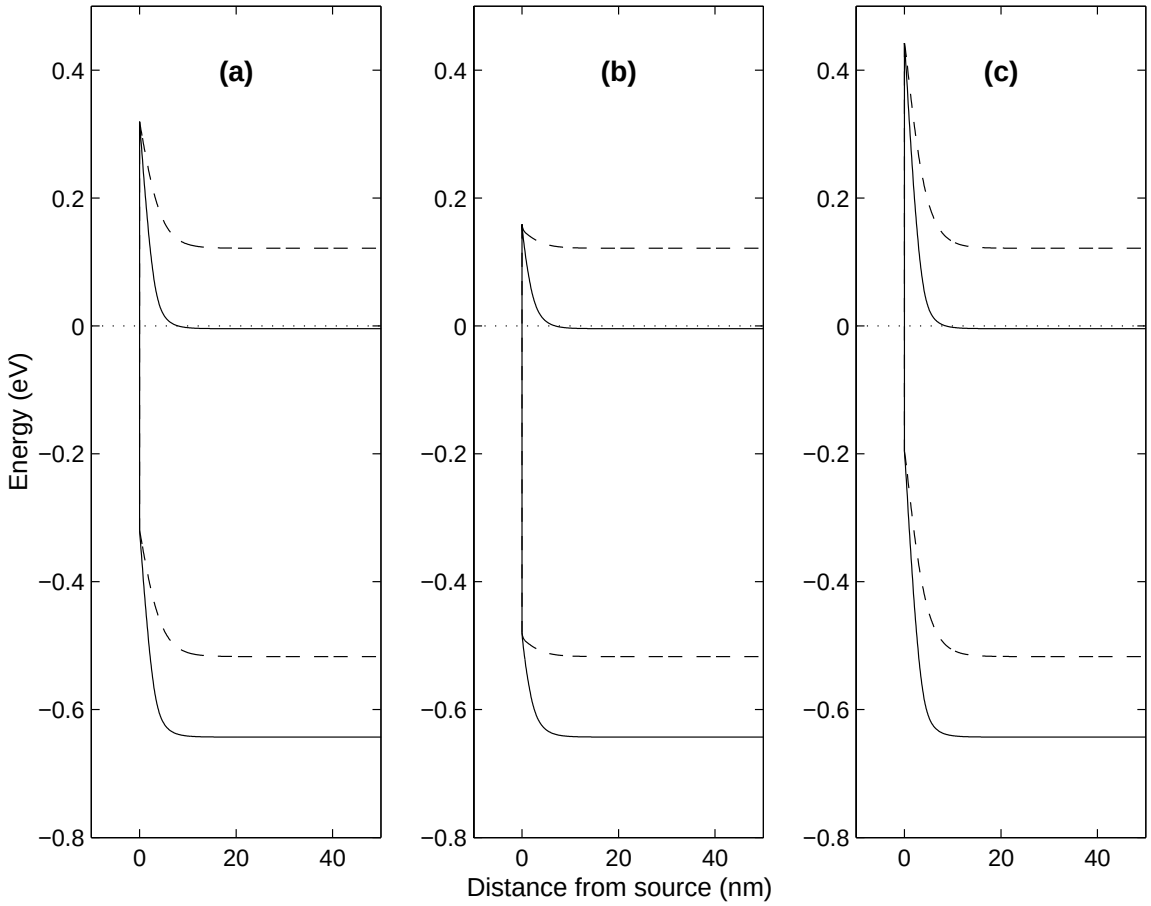

Figure 2: Self-consistent equilibrium energy band diagram near the source for a $(16, 0)$ tube with a 5.6 nm gate dielectric thickness ($R_G/R_T = 10$), and $\Phi_S = \Phi_D$ set to (a) 4.5 eV, (b) 4.33 eV, and (c) 4.63 eV. Data are for $V_{DS} = 0$ V and $V_{GS} = 0.2$ (dashed line) and 0.5 V (solid line). Energies are with respect to the Fermi level (dotted line).

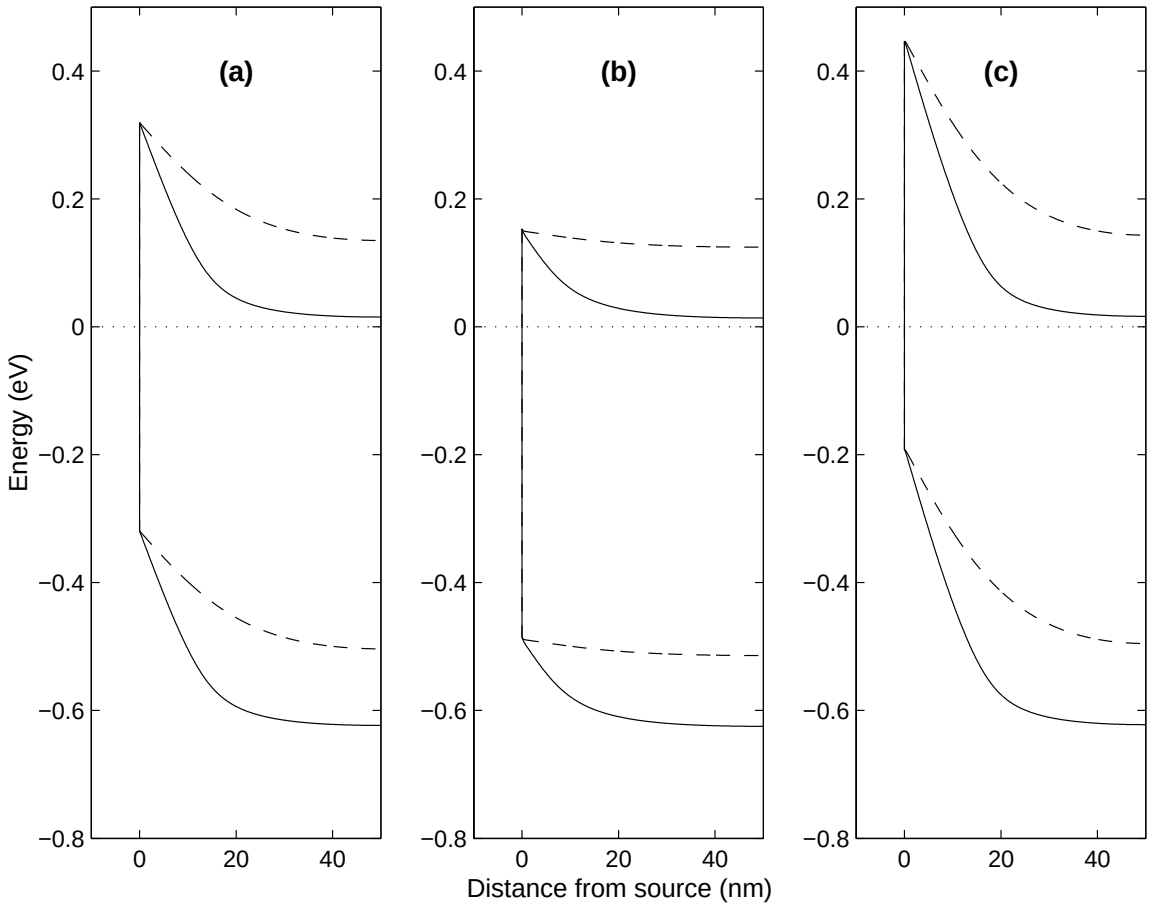

Figure 3: Self-consistent equilibrium energy band diagram near the source for a $(16, 0)$ tube with a 30.9 nm gate dielectric thickness ($R_G/R_T = 50$), and the same sequence of work functions as in Fig. 2, namely: $\Phi_S = \Phi_D$ set to (a) 4.5 eV, (b) 4.33 eV, and (c) 4.63 eV. Data are for $V_{DS} = 0$ V and $V_{GS} = 0.2$ (dashed line) and 0.5 V (solid line). Energies are with respect to the Fermi level (dotted line).

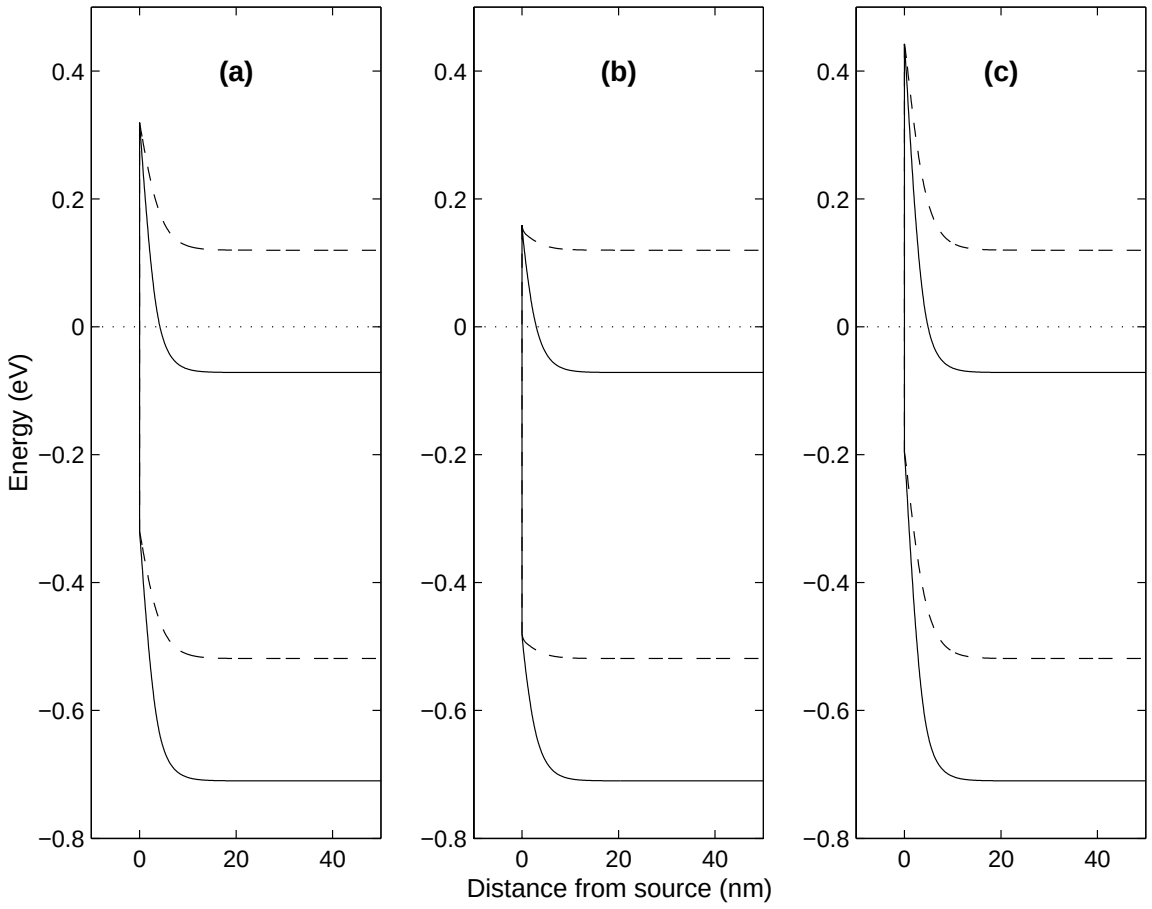

Figure 4: Self-consistent equilibrium energy band diagram near the source for a $(16, 0)$ tube with a 5.6 nm gate dielectric thickness ($R_G/R_T = 10$), a gate dielectric with permittivity 5 times higher than used in Fig. 2, and the same sequence of work functions as in Fig. 2, namely: $\Phi_S = \Phi_D$ set to (a) 4.5 eV, (b) 4.33 eV, and (c) 4.63 eV. Data are for $V_{DS} = 0$ V and $V_{GS} = 0.2$ (dashed line) and 0.5 V (solid line). Energies are with respect to the Fermi level (dotted line).

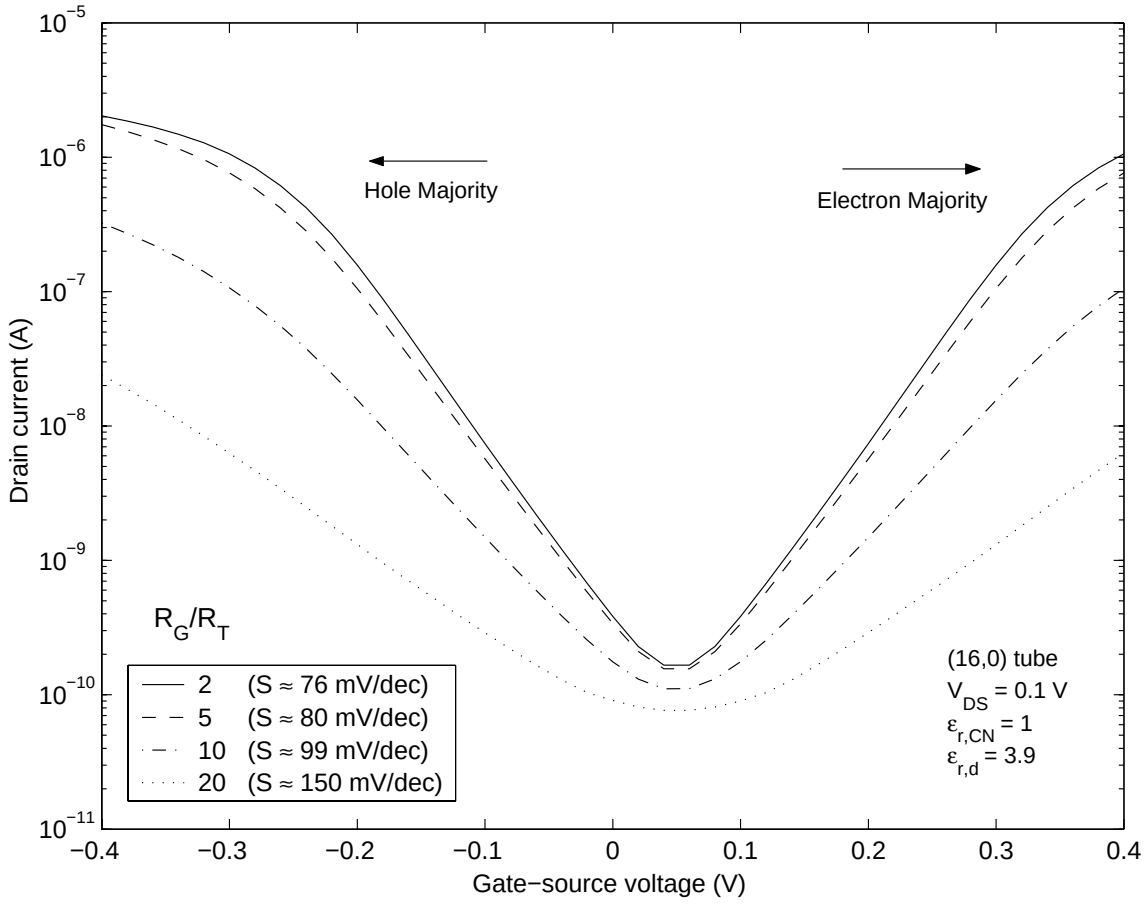

Figure 5: Sub-threshold current for the same tube properties as in Fig. 2(a), but with various ratios of gate radius to tube radius, for $V_{DS} = 0.1\,\mathrm{V}$. Note: the dielectric thickness is $R_G - R_T$.

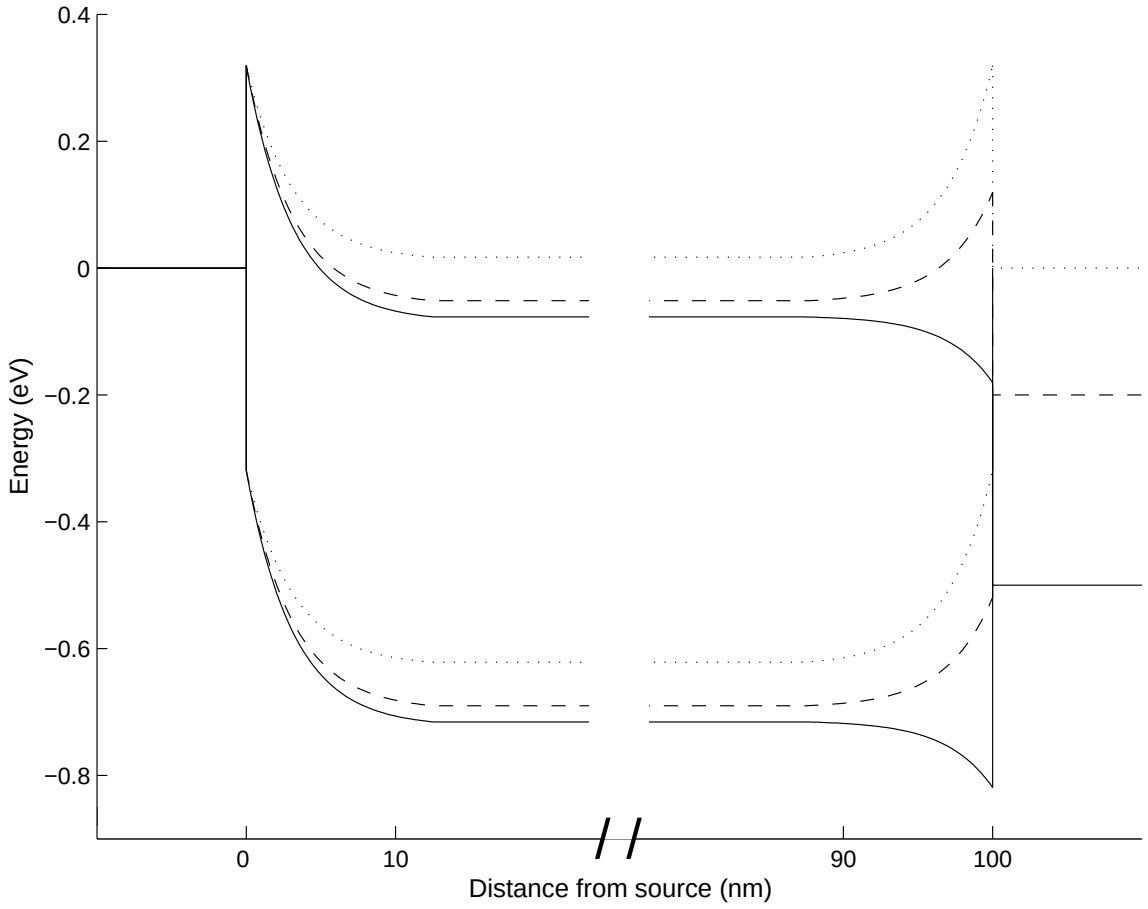

Figure 6: Energy band diagrams for the same tube properties as in Fig. 2(a) for $V_{GS} = 0.3\,\mathrm{V}$ and various V_{DS}: $0\,\mathrm{V}$ (dotted), $0.2\,\mathrm{V}$ (dashed), $0.5\,\mathrm{V}$ (solid). For the equilibrium case the profile is the exact solution of Poisson's equation; for $V_{DS} \neq 0$ the solutions are from Castro's compact model [10], with the base widths of the potential profiles at the source and drain being taken as $2R_G$.

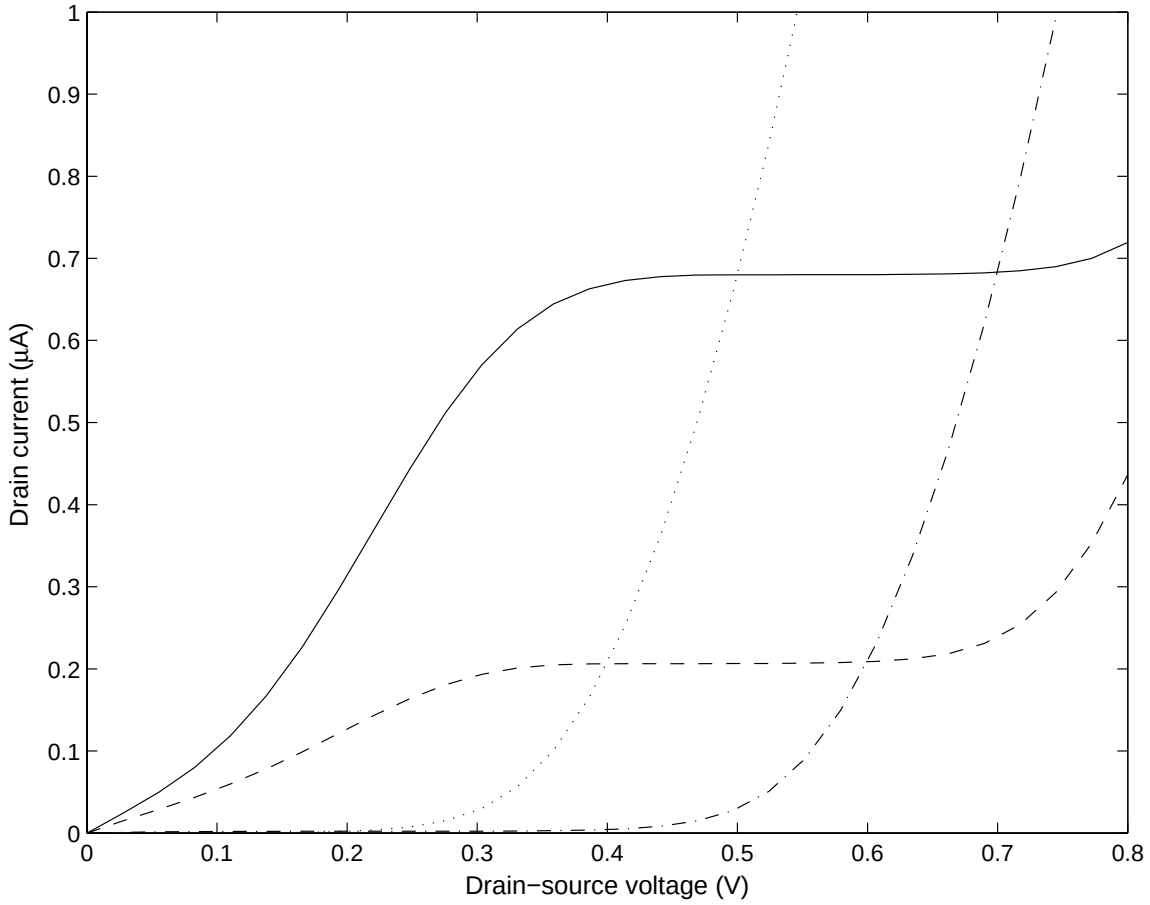

Figure 7: Drain I-V characteristics, as calculated by the method of Ref. [10], for a $(16, 0)$ tube, $R_G/R_T = 10$, $\Phi_S = \Phi_D = 4.5\,\mathrm{eV}$ and various values of V_{GS}: $0\,\mathrm{V}$ (dotted), $0.2\,\mathrm{V}$ (dot-dashed), $0.4\,\mathrm{V}$ (dashed), $0.5\,\mathrm{V}$ (solid).